A Multi-modal Deep Learning Framework for Psoriasis Diagnosis by Integrating Unaffected Fingernail Morphology and Clinical Indicators

1st Xiaoyan Li†
Department of Automation
Tsinghua University
Beijing, China
xiaoyanli629@tsinghua.edu.cn

2nd RuiZhen Liu†
Xiangya Hospital
Central South University
Changsha, China
1806820413@qq.com

3rd Cuicui Jiang†
College of Computer Science
Inner Mongolia University
Hohhot, China
jiancuicui@mail.imu.edu.cn

4th Zijing Chen
School of Clinical Medicine
Tsinghua University
Beijing, China
zijingc@tsinghua.edu.cn

5th Rebecca Lahr
Ann Arbor City
Ann Arbor City
Ann Arbor, America
rlahr@a2gov.org

6th YeHong Kuang*
Xiangya Hospital
Central South University
Changsha, China
yh_927@126.com

7th Liwen Xu*
Furong Laboratory
Central South University
Changsha, China
xuliwen@csu.edu.cn

2025 IEEE International Conference on Bioinformatics and Biomedicine (BIBM) | 979-8-3315-1557-7/25/$31.00 ©2025 IEEE | DOI: 10.1109/BIBM66473.2025.11357204

***Abstract*—Psoriatic arthritis (PsA) is a complex inflammatory disease and a more severe condition of psoriasis (PsO), frequently accompanied by skin and nail lesions. Early differentiation between these conditions is crucial for appropriate treatment selection and improved patient outcomes. Therefore, this study assesses the contribution of the unaffected fingernail indicators and presents PsACasNet, a multi-modal cascaded fusion neural network for effective classification of PsA out of PsO. The framework integrates the clinical phenotypes, protein structural features, and morphology of the unaffected fingernails of patients. PsACasNet implements a biology-driven cascade fusion pathway from molecular (spectral) to morphological (SEM image), and then to clinical indicators. Through comprehensive ablation studies evaluating seven different modal combinations, we demonstrate the effectiveness of our model, which follows a biology-driven molecular-to-morphological-to-clinical fusion pathway. Experimental results show that dual-modal combinations of Clinical+Spectral and Spectral+Image achieve optimal performance (92.0% accuracy), while spectral features alone reach 84.0% accuracy, highlighting the discriminative power of molecular characteristics. The comparison with other traditional machine-learning methods demonstrates the efficiency of our multi-modal fusion strategies. Moreover, through the interpretability analysis of the model, we found that the morphological and protein characteristics of the uninvolved nails have made outstanding contributions to the diagnosis of PsA and can serve as effective biomarkers to promote diagnosis.**

***Index Terms*—Multi-model Fusion, Deep Learning, Psoriasis Diagnosis, Nail Involvement Characteristics**

I. Introduction

PsO and PsA represent significant challenges in dermatology and rheumatology, affecting approximately 2-3% of the global population [1]. PsO is a chronic autoimmune condition characterized by rapid skin cell proliferation, leading to distinctive scaling and inflammation. PsA, a more severe condition, develops in approximately 30% of PsO patients, causing progressive joint damage and significant disability if left untreated [2, 3]. Given the absence of therapeutic interventions capable of reversing joint disability, early identification of patients at high risk for progression from psoriasis to PsA is paramount. However, identifying such patients presents significant challenges, as diagnostic biomarkers for early PsA detection are currently lacking.

Nail psoriasis represents one of the most predictive clinical indicators for PsA development [4]. Psoriasis patients with nail lesions (e.g., pitting, onycholysis, crumbling, discoloration) show higher PsA susceptibility than those without nail involvement [4, 5], though not all PsA patients manifest nail pathology. Current clinical assessment of psoriatic nail changes is limited to visual observation, and it remains unclear whether apparently normal nails possess identical microstructural characteristics in PsO versus PsA patients. As nails consist primarily of keratin [6, 7], their mechanical stability depends critically on: (1) disulfide-bonded keratin chains, (2) peptide-bonded amide I (1620–1640 cm^{-1}) and amide II groups stabilized by hydrogen bonding and β-sheets [8, 9], making these bonds essential for nail quality evaluation.

Currently, the automated diagnostic systems for PsO and PsA face significant challenges. Conventional diagnostic approaches rely on clinical observation, medical history, and laboratory examinations, which are inherently subjective and time-consuming. Moreover, the subtle molecular changes that precede visible symptoms remain largely undetected by conventional methods. The application of artificial intelligence technology has greatly improved the diagnosis and prediction of diseases, but it predominantly focus on single-modal data

† Equal contribution.
* Corresponding Author: Liwen Xu(xuliwen@csu.edu.cn); Yehong Kuang (yh_927@126.com)

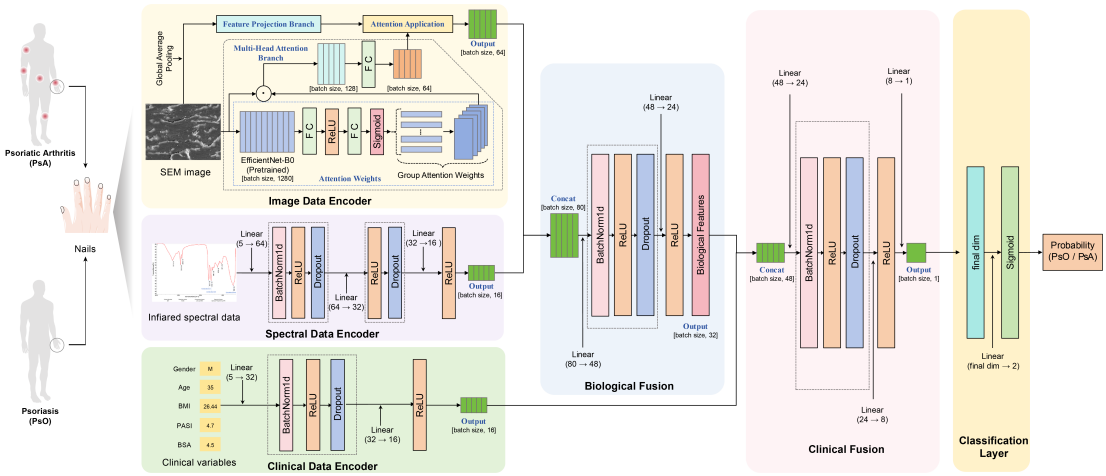

Fig. 1. Overview of the PsACasNet architecture of multi-modal fusion for PsA/PsO classification.

analysis, missing synergistic information across multiple biological scales. Besides, many systems lack interpretability, hindering further promotion and application. Advances in biomedical technology have enabled multi-scale biological data collection and analysis [10]. Integration of clinical phenotypic data, molecular-level spectroscopic information, and cellular morphological characteristics provides a methodology for more accurate early diagnosis [11].

This study focuses on the morphology and keratin structure features of healthy nails, exploring the role of nails in predicting the development of PsA in PsO patients. we develop an enhanced hierarchical multimodal [12] deep learning network, PsACasNet, that integrates multi-scale biomedical data through a biology-driven hierarchical architecture mirroring natural disease progression from molecular to clinical manifestations, providing accurate classification and interpretable results (Fig. 1)

II. MATERIALS AND METHODS

A. Sample collection

Clipped fingernail plates were collected (Nov 2023-Aug 2024) from healthy volunteers, PsO patients with dermatologist-confirmed silvery scales, and PsA patients diagnosed according to the Classification Criteria for Psoriatic Arthritis (CASPAR). CASPAR, established by the international rheumatology community in 2006 [13], provides standardized diagnostic criteria for PsA with high sensitivity and specificity.

All patients with psoriasis were treatment naive for 3 months and excluded for comorbidities or nail infections. Patients with comorbidities such as cancer, hepatitis, renal insufficiency, primary and secondary hyperparathyroidism, osteoporosis, unexplained elevations in alkaline phosphatase, finger injuries, and nail fungal infections were excluded from this study. Unaffected distal segments (1-3 mm) of the right middle fingernail were washed, dried, bagged, and stored at -20°C. Samples were analyzed within one week. Ethics approval (Xiangya Hospital #202308636) and informed consent were obtained.

B. SEM

Scanning electron microscopy (SEM) was conducted using a Czech Tescan MIRA LMS to examine the surface morphology of nail plate samples (both dorsal and ventral sides). To enhance the conductivity of the samples, a thin layer of gold was deposited on their surfaces using ion sputtering coating technology. Observations of the samples were made under a secondary electron (SE) mode at an accelerating voltage of 15 keV.

C. Micro-Fourier Transform Infrared Spectroscopy (FTIR) analysis

Nail samples underwent micro-FTIR (Thermo Nicolet iN10) in Attenuated Total Reflectance (ATR) mode (400–4000 cm^{-1}, 32 scans, 4 cm^{-1} resolution). Post-background scan, spectra were Fourier-transformed and processed via Omnic software (absorbance conversion, baseline correction, smoothing). Peak positions (local maxima) and areas of Amide I/II and Disulfide bands were quantified in Origin 2022 software, using healthy nails as a reference for relative calculations.

D. Model Construction

The psoriasis classification task is formulated as binary classification predicting $y_i \in \{0, 1\}$ for PsA and PsO. Each sample comprises the multi-modal data of clinical characteristics $\mathbf{c}_i \in \mathbb{R}^5$, spectral characteristics $\mathbf{s}_i \in \mathbb{R}^5$ of infrared spectroscopy, and SEM images $\mathbf{I}_i \in \mathbb{R}^{224\times224\times3}$. The objective learns an optimal mapping integrating all modalities:

$$f : (\mathbf{c}_i, \mathbf{s}_i, \mathbf{I}_i) \rightarrow y_i \tag{1}$$

Our hierarchical multi-modal framework uses three encoders: a two-layer network for clinical data, a three-layer network for spectral patterns, and EfficientNet-B0 with attention for SEM images.The multi-modal data were integrated by a two-stage hierarchical fusion that first combines molecular and

morphological features, then integrates clinical information, mirroring the biological progression from molecular alterations to clinical manifestations (Fig. 1).

*1) **Single-mode encoder design**:* Three specialized encoders extract features: a two-layer network for clinical data, a three-layer network for spectral patterns, and EfficientNet-B0 with attention for SEM images.

a) Clinical Data Encoder: Two-layer network processes 5-dimensional clinical features (5→32→16):

$$\mathbf{h}_c = \text{ReLU}(\text{BN}(\mathbf{W}_c^{(2)} \cdot \text{ReLU}(\text{BN}(\mathbf{W}_c^{(1)}\mathbf{c} + \mathbf{b}_c^{(1)})) + \mathbf{b}_c^{(2)})) \tag{2}$$

b) Spectral Data Encoder: Three-layer architecture extracts molecular signatures (5→64→32→16):

$$\begin{aligned}\mathbf{h}_s =& \text{Dropout}(\text{ReLU}(\text{BN}(\mathbf{W}_s^{(3)} \cdot \text{ReLU}(\text{BN}(\mathbf{W}_s^{(2)} \cdot \text{ReLU} \\ & (\text{BN}(\mathbf{W}_s^{(1)}\mathbf{s} + \mathbf{b}_s^{(1)})) + \mathbf{b}_s^{(2)})) + \mathbf{b}_s^{(3)})))\end{aligned} \tag{3}$$

c) Image Encoder: We employ EfficientNet-B0 for its proven effectiveness in biomedical image analysis and optimal balance between computational efficiency and feature extraction capability. EfficientNet-B0 extracts features from 224×224 SEM images:

$$\mathbf{f}_{img} = \text{EfficientNet}(\mathbf{I}), \quad \mathbf{h}_i = \text{GlobalAvgPool}(\mathbf{f}_{img}) \in \mathbb{R}^{1280} \tag{4}$$

Attention mechanism refines features:

$$\mathbf{A} = \text{Softmax}(\frac{\mathbf{Q}\mathbf{K}^T}{\sqrt{d_k}}), \quad \mathbf{h}_{i,att} = \mathbf{A}\mathbf{V} \tag{5}$$

$$\mathbf{h}_i^{final} = \text{Linear}(\mathbf{h}_{i,att}) \in \mathbb{R}^{64} \tag{6}$$

*2) **Hierarchical Fusion Strategy**:* Two-stage biologically-motivated fusion mirrors pathophysiological progression from molecular to clinical manifestations. Our two-stage fusion follows the natural progression from microscopic to macroscopic disease manifestation: molecular alterations precede morphological changes, which ultimately manifest as clinical symptoms.

a) Stage 1: Biological Feature Fusion: Combines spectral and image features:

$$\mathbf{h}_{bio} = \text{ReLU}(\text{BN}(\mathbf{W}_{bio}[\mathbf{h}_s; \mathbf{h}_i] + \mathbf{b}_{bio})) \tag{7}$$

where $[\mathbf{h}_s; \mathbf{h}_i] \in \mathbb{R}^{80}$ creates unified molecular-morphological representation $\mathbf{h}_{bio} \in \mathbb{R}^{32}$.

b) Stage 2: Clinical Integration: Integrates biological representation with clinical features:

$$\mathbf{h}_{final} = \text{ReLU}(\text{BN}(\mathbf{W}_{final}[\mathbf{h}_{bio}; \mathbf{h}_c] + \mathbf{b}_{final})) \tag{8}$$

*3) **Biological Significance of the Two-Stage Hierarchical Architecture**:* Our hierarchical fusion architecture models biological causality in psoriatic conditions. Stage 1 (Eq. 7) captures molecular alterations driving morphological changes, while Stage 2 (Eq. 8) integrates biological evidence with patient phenotype for diagnosis. This approach improves accuracy while providing clinically interpretable insights aligned with pathophysiological knowledge.

E. Loss Function Design

Our loss function balances classification accuracy, generalization, and interpretability through three components: binary cross-entropy for PsA/PsO classification, L2 regularization to prevent overfitting, and attention regularization for interpretable patterns.

a) Primary Classification Loss: Binary cross-entropy handles class imbalance:

$$\mathcal{L}_{cls} = -\frac{1}{N}\sum_{i=1}^{N}[y_i \log(\hat{y}_i) + (1 - y_i)\log(1 - \hat{y}_i)] \tag{9}$$

b) Regularization Loss: L2 regularization prevents overfitting:

$$\mathcal{L}_{reg} = \lambda \sum_{\theta \in \Theta} ||\theta||_2^2 \tag{10}$$

where $\lambda = 1 \times 10^{-4}$ controls regularization strength.

c) Attention Regularization: Encourages focused, interpretable attention:

$$\mathcal{L}_{att} = \alpha \sum_{i=1}^{N} ||\mathbf{A}_i||_1 + \beta \sum_{i=1}^{N} H(\mathbf{A}_i) \tag{11}$$

with sparsity term ($\alpha = 0.01$) and entropy term ($\beta = 0.001$).

The total loss combines all components:

$$\mathcal{L}_{total} = \mathcal{L}_{cls} + \mathcal{L}_{reg} + \mathcal{L}_{att} \tag{12}$$

F. Training Strategy and Optimization

The model was trained on 124 patients using a stratified split ratio of approximately 64:16:20 to ensure balanced representation of PsA and PsO cases across sets: 79 patients for training, 20 for validation, and 25 for testing. This stratified splitting approach maintained consistent disease prevalence across all datasets to prevent sampling bias. The model used Adam optimizer($\beta_1 = 0.9$, $\beta_2 = 0.999$) with initial learning rate 1×10^{-4} and cosine annealing scheduler. Training used batch size 8 over 200 epochs with early stopping (patience 20). Training used batch size 8 over 200 epochs with early stopping (patience 20), as smaller batch sizes demonstrated superior convergence and generalization compared to larger alternatives (16, 24). The loss function combined binary cross-entropy, L2 regularization ($\lambda = 1 \times 10^{-4}$), and attention regularization ($\alpha = 0.01$, $\beta = 0.001$). Data augmentation included random flipping, rotation ($\pm 15°$), and intensity normalization for images, with standardization for clinical/spectral features. EfficientNet-B0 used ImageNet pre-trained weights with dropout (p = 0.2) in the spectral encoder, achieving 92.0% test accuracy. In this project, we utilize the EfficientNet model due to its superior accuracy-efficiency trade-off and significantly reduced computational requirements [14].

G. Ablation Study Design

To systematically evaluate the contribution of each modality and the effectiveness of the hierarchical fusion strategy, we designed a comprehensive ablation study with seven distinct configurations, as detailed in Table I. This study, through

TABLE I
ABLATION STUDY CONFIGURATION DESIGN

Model Specs	Modalities	Model Formulation	Rationale & Objective
Clinical	Clinical	$f_1(\mathbf{c}) \rightarrow y$	Establish baseline performance using only structured clinical data.
Spectral	Spectral	$f_2(\mathbf{s}) \rightarrow y$	Evaluate the independent discriminative power of molecular features.
Image	Image	$f_3(\mathbf{I}) \rightarrow y$	Assess the independent contribution of morphological image features.
Clinical + Spectral	Clinical, Spectral	$f_4(\mathbf{c}, \mathbf{s}) \rightarrow y$	Evaluate the synergistic effect of combining clinical and molecular data.
Clinical + Image	Clinical, Image	$f_5(\mathbf{c}, \mathbf{I}) \rightarrow y$	Assess the synergy between clinical context and morphological features.
Spectral + Image	Spectral, Image	$f_6(\mathbf{s}, \mathbf{I}) \rightarrow y$	Test the performance of the first-level biological feature fusion.
PsACasNet	Clinical, Spectral, Image	$f_7(\mathbf{c}, \mathbf{s}, \mathbf{I}) \rightarrow y$	Evaluate the full hierarchical fusion model with all three modalities.

configurations C1-C7, allows us to isolate the performance of individual modalities and their combinations, providing clear insights into their synergistic and independent contributions.

H. Statistical Analysis

For continuous variables, statistical differences were estimated by the Wilcoxon rank-sum test. Categorical variables were compared using the Chi-square test. Correlation analysis was performed using Spearman's method. All statistical analyses were two-sided.

III. RESULTS

A. Patients Characteristics

We first conducted a comparative analysis of baseline demographic characteristics, clinical features, and nail keratin profiles between collected cohorts of PsO and PsA patients. The results revealed no statistically significant differences in baseline characteristics such as gender, age, or body mass index (BMI) between the two groups (Fig. 2A-C). However, significant differences in the Psoriasis Area and Severity Index (PASI) and the percentage of Body Surface Area (BSA) were observed, which align with the disease severity between groups (Fig. 2D-E). Furthermore, the nail keratin structural features based on the micro-Fourier-transform infrared (FTIR) spectroscopy demonstrate more distinct distributions, including the assessment of amide I bond, amide II bond, and disulfide bonds, suggesting that they may possess stronger independent discriminative power for classification (Fig. 2F-J).

B. Model Performance Analysis

To assess the contribution of features of unaffected fingernails in classifying PsA, we performed comprehensive ablation experiments (Table I). Training and validation curves demonstrate distinct convergence patterns across configurations. Spectral-based models show rapid convergence with stable validation performance, while Image models exhibit more volatile training dynamics (Fig. 3A). The PsACasNet configuration shows gradual improvement with occasional overfitting, highlighting the challenge of optimizing complex multi-modal architectures with limited data. The hierarchical

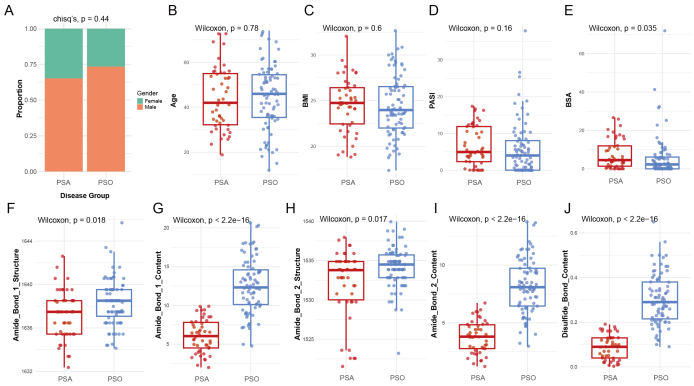

Fig. 2. Comparison of the clinical characteristics between PsA and PsO patients. **(A)** Differences in the proportion of gender. Comparison of the distribution of the age **(B)**, BMI **(C)**, PASI **(D)**, BSA **(E)**, amide I bond structure **(F)**, amide I bond content **(G)**, amide II bond structure **(H)**, amide II bond content **(I)**, and disulfide bonds content **(J)**.

fusion strategy of PsACasNet implements a biologically motivated two-stage integration process that mirrors the pathophysiological progression from molecular changes to clinical manifestations in psoriatic conditions.

Further, the diagnostic performance of different model configurations was evaluated using Receiver Operating Characteristic (ROC) curves (Fig. 3B). The dual-modal Clinical+Spectral configuration achieved the highest AUC of 0.993, followed by Spectral+Image at 0.979. Notably, the Spectral model alone reached an AUC of 0.958, while the Clinical model showed limited discriminative power. The PsACasNet fusion model achieved an AUC of 0.965, demonstrating the effectiveness of our integrated approach (Table II).

Feature representation analysis was conducted using UMAP (Uniform Manifold Approximation and Projection) to visualize learned embeddings across multiple modalities (Fig. 3C). Prior to UMAP visualization, PCA was conducted on the embeddings extracted from the final linear layer to reduce dimensionality while preserving key feature relationships.

The UMAP projections revealed distinct clustering patterns, with spectral features showing the strongest class separation

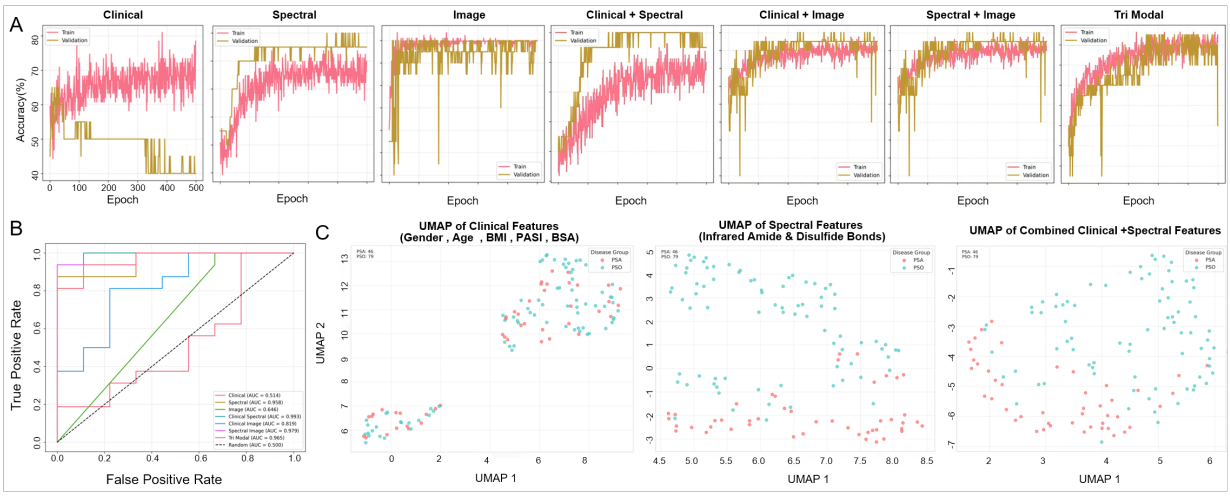

Fig. 3. Performance Evaluation of Different Multi-modal Fusion Strategies. **(A)** Accuracy curves of the training and validation set. **(B)** ROC curves of different multi-modal fusion strategies. **(C)** Umap of the PCA analysis results of clinical features (left), spectral features (middle), and combined features (right).

TABLE II
PERFORMANCE EVALUATION OF DIFFERENT MULTI-MODAL FUSION STRATEGIES AND PREVIOUS MODELS

Model	Acc.	Prec.	Rec.	F1	AUC
Ablation Configurations					
Clinical+Spectral	92.0	93.8	93.8	93.8	0.993
Spectral+Image	92.0	93.8	93.8	93.8	0.979
PsACasNet	88.0	84.2	100.0	91.4	0.965
Spectral	84.0	87.5	87.5	87.5	0.958
Clinical+Image	76.0	72.7	100.0	84.2	0.819
Image	72.0	71.4	93.8	81.1	0.646
Clinical	52.0	64.3	56.2	60.0	0.514
Traditional ML Models					
SVM	65.8	66.7	91.7	77.2	0.634
Log. Reg.	63.2	63.2	100.0	77.4	0.446
Random Forest	55.3	62.1	75.0	67.9	0.551
KNN	52.6	60.7	70.8	65.4	0.579
Naive Bayes	52.6	61.5	66.7	64.0	0.455
Decision Tree	47.4	58.3	58.3	58.3	0.435

capability.

In addition, we compared our model with the traditional machine-learning methods, including support vector machine (SVM), logistic regression, random forest, K-nearest neighbors, naive bayes, and decision tree. The accuracy (Acc.), precision (Prec.), recall (Rec.), F1-score, and AUC are comprehensively compared, and our model outperformed the above traditional methods, further suggesting the effectiveness of the multi-modal fusion in PsO classification (Table II).

C. Model Interpretability

To enhance interpretability, we analyzed different modalities' contributions. Spearman's correlation analysis (Fig. 4A) revealed strong correlation between PASI and BSA scores ($\rho = 0.84$), while demographic and clinical indicators showed weak correlations with spectral features. Strong intra-correlations existed among spectral features (Amide bond I and II: $\rho = 0.99$; disulfide bond: $\rho = 0.80$), supporting their integration in our multi-modal framework.

SHAP analysis revealed nail keratin's molecular features as the strongest contributors to classification (Fig. 4B). Disulfide bond content was the primary discriminative feature (mean |SHAP| = 0.1799), followed by amide bond markers (Amide Content II: 0.1057; I: 0.0725, Fig. 4B). Clinical features showed modest influence, with BSA (mean |SHAP| = 0.0267) and age (mean |SHAP| = 0.0239) as leading parameters (Fig. 4B).

IV. DISCUSSION

This study validates the efficacy of a biologically inspired hierarchical fusion network for precise and interpretable diagnosis of PsA. We innovatively proposed PsACasNet, integrating molecular features with morphological characteristics and clinical phenotypes. Through systematic ablation studies, we found dual-modal combinations (Clinical+Spectral and Spectral+Image) achieved superior accuracy (92.0%), primarily due to the strong discriminative power of spectral features (84.0%). The hierarchical PsACasNet achieved 88.0% accuracy, with performance limitations likely due to information redundancy and increased model complexity. SHAP analysis revealed significant molecular and clinical determinants of PsA diagnosis. Our study's limitations include moderate dataset size and need for external validation. Future work will focus on data expansion and computational optimization to enhance the model's generalizability.

V. CONCLUSION

This research successfully developed a hierarchical multi-modal fusion deep learning network for high-accuracy psoriasis classification. Key findings demonstrate the strong discriminative power of spectral features, and their integration with the clinical and image data. Scientifically, it offers a

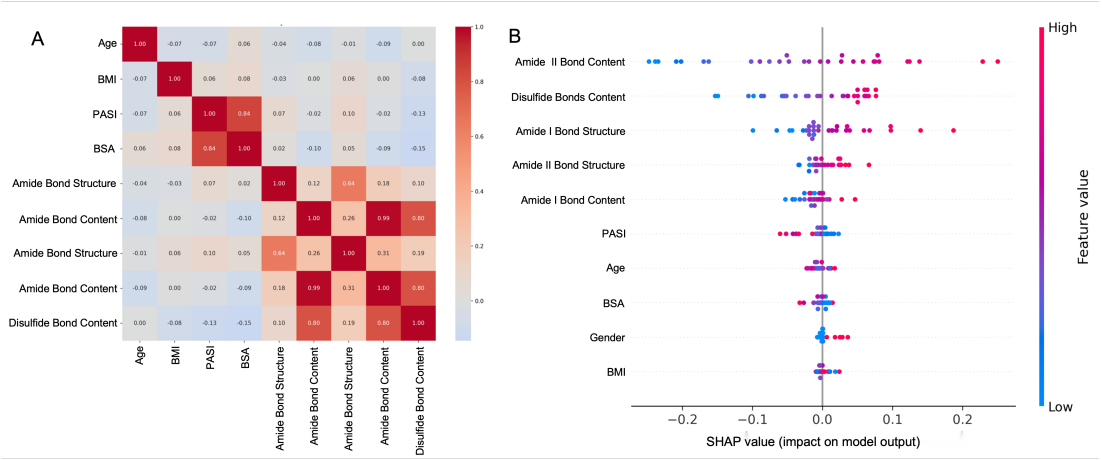

Fig. 4. Correlation and importance of features through the interpretability analysis. **(A)** Correlation among the demographic, clinical, and nail keratin features across patients. **(B)** SHAP analysis revealed the global interpretability for multiple features.

novel biology-driven theoretical framework, systematic ablation methodology, validated multi-modal diagnostic utility, and a foundational technical reference for related AI-driven disease diagnosis. Project code is available at GitHub.

Acknowledgment

This work was supported by the National Key R&D Program of China (2023YFC2508100) and the Young Elite Scientists Sponsorship Program by CAST (2023QNRC001).

References

[1] Alen Zabotti, Gabriele De Marco, Laure Gossec, Xenofon Baraliakos, Daniel Aletaha, Annamaria Iagnocco, Paolo Gisondi, Peter V Balint, Heidi Bertheussen, Wolf-Henning Boehncke, et al. Eular points to consider for the definition of clinical and imaging features suspicious for progression from psoriasis to psoriatic arthritis. *Annals of the rheumatic diseases*, 82(9):1162–1170, 2023.

[2] Oliver FitzGerald, Alexis Ogdie, Vinod Chandran, Laura C Coates, Arthur Kavanaugh, William Tillett, Ying Ying Leung, Maarten deWit, Jose U Scher, and Philip J Mease. Psoriatic arthritis. *Nature reviews Disease primers*, 7(1):59, 2021.

[3] R Baran and B Sigurgeirsson. Psoriatic nail disease, a predictor of psoriatic arthritis. *British Journal of Dermatology*, 171(5), 2014.

[4] Shiqi Wang, Jianjian Zhu, Ping Wang, Jing Dong, Yanling Li, Dongmei Shi, Huiping Wang, Xi Huang, Xibao Zhang, Bo Yu, et al. Nail psoriasis in china: a prospective multicentre study. *Journal of the European Academy of Dermatology and Venereology*, 38(3):549–556, 2024.

[5] Adam Reich and Jacek C Szepietowski. Health-related quality of life in patients with nail disorders. *American journal of clinical dermatology*, 12(5):313–320, 2011.

[6] Takashi Kitahara and Hideoki Ogawa. The extraction and characterization of human nail keratin. *Journal of dermatological science*, 2(6):402–406, 1991.

[7] D De Berker, F Wojnarowska, L Sviland, GE Westgate, RPR Dawber, and IM Leigh. Keratin expression in the normal nail unit: markers of regional differentiation. *British Journal of Dermatology*, 142(1):89–96, 2000.

[8] Min Kyung Shin, Tae In Kim, Wan Sun Kim, Hun-Kuk Park, and Kyung Sook Kim. Changes in nail keratin observed by raman spectroscopy after nd: Yag laser treatment. *Microscopy Research and Technique*, 80(4):338–343, 2017.

[9] Praveer Sihota, Ram Naresh Yadav, Vandana Dhiman, Sanjay Kumar Bhadada, Vishwajeet Mehandia, and Navin Kumar. Investigation of diabetic patient's fingernail quality to monitor type 2 diabetes induced tissue damage. *Scientific reports*, 9(1):3193, 2019.

[10] Yingbo Cui, Chenchen Peng, Zeyu Xia, Canqun Yang, and Yifei Guo. A survey of sequence-to-graph mapping algorithms in the pangenome era. *Genome Biology*, 26(1):138, 2025.

[11] Min Chen, Shiwen Mao, and Yunhao Liu. Big data: A survey. *Mobile networks and applications*, 19(2):171–209, 2014.

[12] Xiang Zhang, Lina Yao, Chaoran Huang, Tao Gu, Zheng Yang, and Yunhao Liu. Deepkey: A multimodal biometric authentication system via deep decoding gaits and brainwaves. *ACM Transactions on Intelligent Systems and Technology (TIST)*, 11(4):1–24, 2020.

[13] William Taylor, Dafna Gladman, Philip Helliwell, Antonio Marchesoni, Philip Mease, and Herman Mielants. Classification criteria for psoriatic arthritis: development of new criteria from a large international study. *Arthritis & Rheumatism: Official Journal of the American College of Rheumatology*, 54(8):2665–2673, 2006.

[14] Mingxing Tan and Quoc Le. Efficientnet: Rethinking model scaling for convolutional neural networks. In *International conference on machine learning*, pages 6105–6114. PMLR, 2019.